Molecular Therapy
Oncology
Original Article

Engineered oncolytic virus OH2-FLT3L enhances antitumor immunity via dendritic cell activation

Duo Wan,[1,6] Qi Zhang,[1,6] Zhenrong Yang,[2] Xiaoli Zhang,[1] Peipei Xie,[1] Shujun Cheng,[1] Libin Xu,[3] Binlei Liu,[4] Kaitai Zhang,[1] and Wen Zhang[5]

[1]State Key Laboratory of Molecular Oncology, Department of Etiology and Carcinogenesis, National Cancer Center/National Clinical Research Center for Cancer/Cancer Hospital, Chinese Academy of Medical Sciences and Peking Union Medical College, Beijing 100021, China; [2]Department of Gastric Surgery, Fujian Medical University Union Hospital, Fuzhou 350001, China; [3]Department of Orthopedic Surgery, National Cancer Center/National Clinical Research Center for Cancer/Cancer Hospital, Chinese Academy of Medical Sciences and Peking Union Medical College, Beijing 100021, China; [4]National "111" Center for Cellular Regulation and Molecular Pharmaceutics, Key Laboratory of Fermentation Engineering (Ministry of Education), Hubei Provincial Cooperative Innovation Center of Industrial Fermentation, College of Bioengineering, Hubei University of Technology, Wuhan 430068, China; [5]Department of Immunology, National Cancer Center/National Clinical Research Center for Cancer/Cancer Hospital, Chinese Academy of Medical Sciences and Peking Union Medical College, Beijing 100021, China

The combination of oncolytic viruses (OVs) with other immunotherapies, such as immunostimulatory therapies, is a current research hotspot; however, optimizing their therapeutic potential remains to be fully explored. Here, we designed a novel oncolytic herpes simplex virus 2 expressing Fms-like tyrosine kinase 3 ligand (OH2-FLT3L), which induces an antitumor cytotoxic T cell immune response by activating dendritic cells (DCs). We found that OH2-FLT3L specifically infects tumor cells, induces immunogenic cell death (ICD), and releases a large number of tumor-specific antigens, which bound to danger signals and facilitated antigenic cross-presentation by DCs, significantly enhancing T cell activation and function. Experimental results showed that OH2-FLT3L significantly increased the proportion of activated DCs, enhanced the antitumor immune response, and effectively converted "cold" tumors into "hot" tumors. In addition, when combined with anti-PD-1 antibody, OH2-FLT3L further enhanced therapeutic efficacy. In conclusion, OH2-FLT3L, as a novel oncolytic virus, demonstrates the potential to enhance antitumor immune responses through DC activation.

INTRODUCTION

Over the past 2 decades, cancer immunotherapy (CIT) has made significant progress and has become an effective treatment for various types of tumors, gaining widespread clinical attention.[1–3] Despite the increasing number of cancer patients benefiting from immunotherapy, a considerable portion of patients do not respond clinically to these treatments.[4] This therapeutic challenge is largely attributed to tumor cells hijacking host mechanisms to create a niche for themselves, known as the tumor microenvironment (TME), which they gradually manipulate to shift from an antitumor to a pro-tumor response.[5,6] Specifically, many tumors exhibit a non-inflammatory TME characterized by low T cell infiltration, referred to as the immune desert phenotype or "cold tumors," which renders them unresponsive to immune checkpoint blockade.

One promising strategy to overcome these challenges is to convert "cold tumors" into "hot tumors" that respond more robustly to CIT. Dendritic cells (DCs), as crucial antigen-presenting cells (APC), play a central role in initiating antitumor immune responses by capturing tumor antigens and migrating to tumor-draining lymph nodes (TDLNs)[7–9]; however, the immunosuppressive factors in the TME often impair DC function, thereby weakening the effectiveness of the antitumor immune response.[10,11] To enhance the function of DCs and their antitumor effects, Fms-like tyrosine kinase 3 ligand (FLT3L), a key cytokine in promoting DC proliferation and

Received 25 November 2024; accepted 18 March 2025;
https://doi.org/10.1016/j.omton.2025.200975.

[6]These authors contributed equally

Correspondence: Binlei Liu, National "111" Center for Cellular Regulation and Molecular Pharmaceutics, Key Laboratory of Fermentation Engineering (Ministry of Education), Hubei Provincial Cooperative Innovation Center of Industrial Fermentation, College of Bioengineering, Hubei University of Technology, Wuhan 430068, China.
E-mail: liubl@hbut.edu.cn
Correspondence: Kaitai Zhang, State Key Laboratory of Molecular Oncology, Department of Etiology and Carcinogenesis, National Cancer Center/National Clinical Research Center for Cancer/Cancer Hospital, Chinese Academy of Medical Sciences and Peking Union Medical College, Beijing 100021, China.
E-mail: zhangkt@cicams.ac.cn
Correspondence: Wen Zhang, National "111" Center for Cellular Regulation and Molecular Pharmaceutics, Key Laboratory of Fermentation Engineering (Ministry of Education), Hubei Provincial Cooperative Innovation Center of Industrial Fermentation, College of Bioengineering, Hubei University of Technology, Wuhan 430068, China.
E-mail: zhangwen@cicams.ac.cn

maturation,[12] has been tested in clinical trials for certain solid tumors. However, its rapid degradation limits clinical benefits,[13–15] making the search for an effective delivery vector critical. Oncolytic viruses (OVs) induce immunogenic cell death (ICD) in tumor cells, releasing damage-associated molecular patterns (DAMPs) and pathogen-associated molecular patterns (PAMPs), which recruit and activate innate immune cells such as macrophages and DCs, further promoting the activation of tumor-specific T cells in the TME,[16–18] thus providing a promising solution. Despite demonstrating efficacy and safety in multiple clinical trials,[19,20] including the only Food and Drug Administration-approved T-VEC, the efficacy of OVs as monotherapies remains limited, highlighting the need for combination therapies.

To address these limitations, we developed a novel engineered oncolytic herpes simplex virus type 2 (OH2), OH2-FLT3L, which triggers systemic tumor regression by activating DCs and enhancing the function of antigen-specific cytotoxic T cells. By delivering FLT3L directly to the tumor site using an oncolytic herpesvirus, OH2-FLT3L not only enhances the activation of APCs but also induces a robust cytotoxic T cell response. Our study indicates that OH2-FLT3L can reshape the TME by increasing the proportion of activated CD8+ T cells, thereby enhancing the therapeutic efficacy of immune checkpoint inhibitors (ICIs). Overall, our work provides new insights and methods for the application of engineered OVs in CIT, revealing their potential to enhance antitumor immune responses.

RESULTS

Construction of the OH2-FLT3L

The OH2-FLT3L was constructed by deleting the ICP34.5 and ICP47 genes, which are known to regulate neurotoxicity and antigen presentation, respectively (Figure 1A).[21] The FLT3L gene was inserted into the OH2 genome using CRISPR-Cas9 technology (Figures S1A–S1C). We also evaluated the oncolytic activity of OH2 and OH2-FLT3L at three different multiplicities of infection (MOIs), and the results showed no significant difference in viral infection or oncolytic activity between the two viruses (Figure 1B).

Additionally, ELISA analysis of culture supernatants revealed no detectable FLT3L in the OH2 group, while the OH2-FLT3L group exhibited significant FLT3L secretion, confirming robust FLT3L expression in OH2-FLT3L (Figure S1D).

OH2-FLT3L oncolysis releases proteome and DAMPs

To verify whether OH2-FLT3L induces ICD, we analyzed two cell lines: 4T1 (a murine triple-negative breast cancer cell line) and CT26 (a murine colorectal cancer cell line) for the release of DAMPs and tumor antigens. Silver staining and western blot analysis of culture supernatants revealed that OH2-FLT3L infection significantly increased the release of DAMPs, including ATPase, HSP70, HMGB1, and HSPA14, particularly at 48 h post-infection (hpi) (Figures 1C–1E). These results confirmed that OH2-FLT3L-induced tumor cell lysis effectively released the tumor cell proteome and DAMPs, effectively inducing ICD. A similar pattern of DAMPs release was observed in OH2-infected cells, suggesting that FLT3L's primary effect lies in enhancing immune activation, rather than directly influencing ICD induction (Figures S1E and S1F).

OH2-FLT3L activates dendritic cells

DAMPs in the OH2-FLT3L oncolytic products act as danger signals, recognized by innate immune PRRs, which recruit and activate APCs, particularly DCs, to initiate antitumor immune responses. FLT3L is a key growth factor for the differentiation of DCs, playing a critical role in the differentiation and proliferation of progenitor cells into conventional dendritic cells (cDCs) and plasmacytoid DCs (pDCs) in the bone marrow. To assess the effect of OH2-FLT3L on DC activation, supernatants from CT26 cells infected with OH2-FLT3L for 48 hpi (referred to as "oncolysate") were co-cultured with mouse bone marrow-derived DCs (BMDCs) for 24 h. Untreated immature DCs (iDCs) and lipopolysaccharide (LPS)-induced mature DCs (mDCs) served as negative and positive controls, respectively. DCs induced by the oncolysate of unmodified OH2 virus were used as a control group to compare the activation phenotype of DCs.

Co-culture with OH2-FLT3L oncolysate significantly increased the percentage of DCs expressing MHC II and the costimulatory/activation markers CD40, CD80, and CD86 (Figures 2A and S2), while the production of cytokines interleukin (IL)-12 and tumor necrosis factor (TNF)-α was markedly elevated (Figures 2B and 2C). Additionally, DCs induced by OH2 oncolysate exhibited increased costimulatory/activation markers and cytokine secretion compared with iDCs, although the activation was less pronounced compared with OH2-FLT3L oncolysate. This suggested that the presence of FLT3L in the modified OV contributed to DC activation. These data indicated that OH2-FLT3L, through direct viral infection and the action of FLT3L, significantly enhanced DC maturation and activation.

OH2-FLT3L oncolysate-treated DCs induce antigen-specific cytotoxic T cells *in vitro*

Thus far, our experiments have shown that OH2-FLT3L effectively destroys tumor cells, releases the tumor cell proteome, and induces DC activation. To assess whether OH2-FLT3L oncolysate-activated DCs can effectively induce CTLs *in vitro*, we performed a DC-T cell co-culture assay. BMDCs treated with OH2-FLT3L oncolysate were co-cultured with autologous T cells to determine their ability to capture and present tumor antigens (Figure 2D).

Results showed that T cells co-cultured with OH2-FLT3L oncolysate-induced DCs exhibited significantly higher cytotoxicity against syngeneic CT26 cells at different effector-to-target ratios (E:T, 5:1, 10:1, 20:1) compared with untreated iDCs and OH2-treated DCs, while no significant cytotoxicity was observed against irrelevant 4T1 cells (Figures 2E, S3A, and S3B). This tumor-specific killing was further supported by elevated levels of interferon (IFN)-γ and Granzyme B secreted by T cells in the CT26-targeted co-culture system (Figures 2F and 2G).

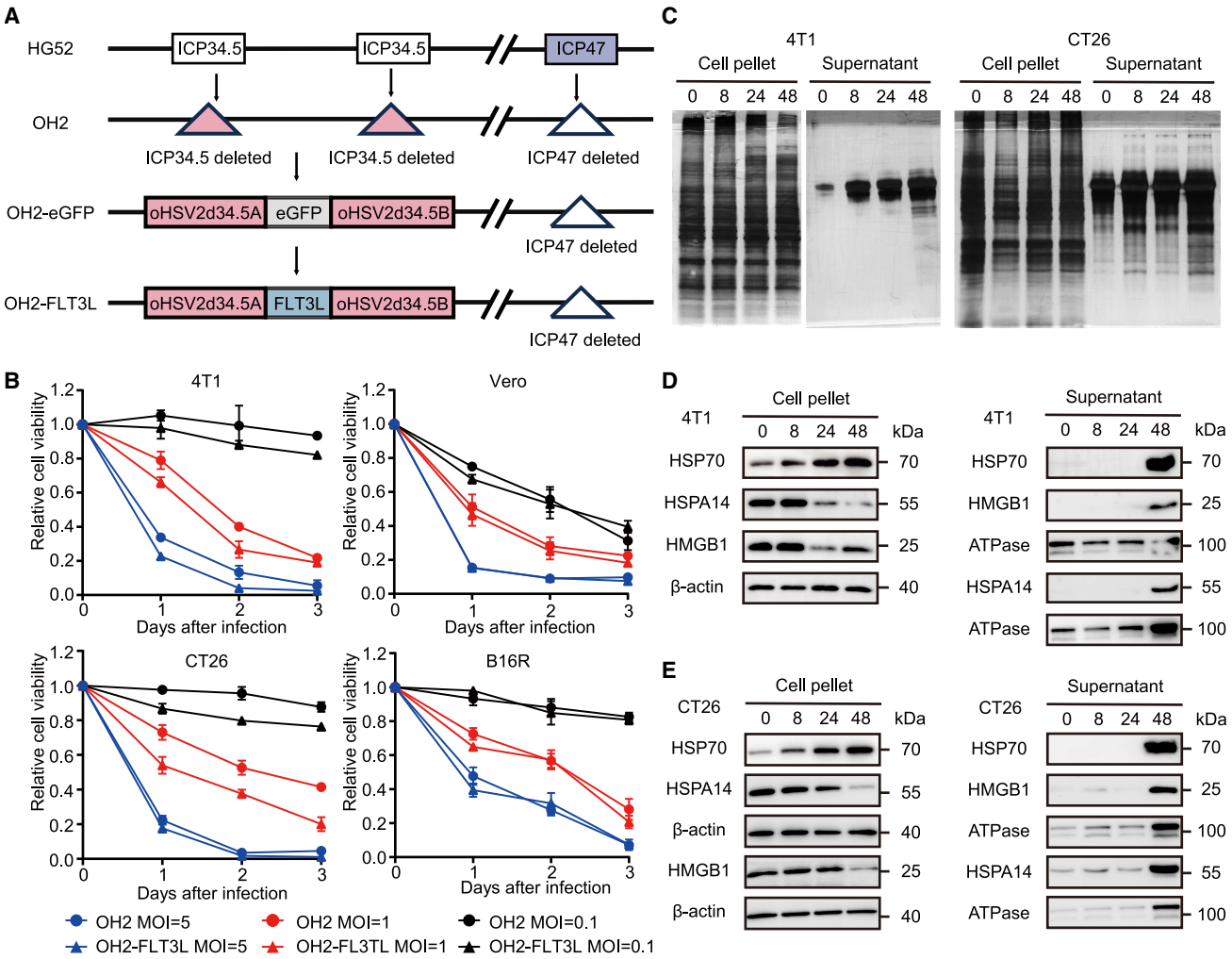

Figure 1. Construction of OH2-FLT3L and release of proteomics and DAMPs during oncolysis

(A) Schematic representation of OH2 and OH2-FLT3L structures. Both OH2 and OH2-FLT3L were derived from the HG52 laboratory strain, with deletions of the ICP34.5 and ICP47 genes. (B) Infection of 4T1, Vero, CT26, and B16R cells was conducted using either OH2 or OH2-FLT3L within the specified time frame. $n = 3$ samples per group, with error bars representing the standard error of the mean (SEM). (C) Following infection of 4T1 and CT26 cells with OH2-FLT3L at 0, 8, 24, and 48 hpi, silver staining was performed on the cell pellets and corresponding supernatants. (D and E) Protein blot analysis of various DAMPs and ATPase was conducted on the cell pellets and corresponding supernatants following infection of 4T1 and CT26 cells with OH2-FLT3L at 0, 8, 24, and 48 hpi. Equal amounts of protein (20 μg) were loaded into the gels. All experiments were repeated three times, and one representative series was presented.

In conclusion, these results demonstrated that DCs treated with OH2-FLT3L oncolysate effectively activated T cells and enhanced their tumor-specific cytotoxicity. Additionally, the increased secretion of IFN-γ and Granzyme B further confirmed the significant enhancement of T cell cytotoxic potential.

OH2-FLT3L induces antitumor immunity in immunocompetent 4T1 and CT26 mouse models

Based on the previous findings that OH2-FLT3L effectively activated DCs and induced CTLs *in vitro*, we next investigated its efficacy *in vivo* using a subcutaneous CT26 tumor model in BALB/c mice (Figure 3A). One week after tumor inoculation, mice were divided into three treatment groups: PBS control, OH2 treatment, and OH2-FLT3L treatment (n = 5–11 per group). As shown in Figures 3B and 3C, both the OH2 ($p < 0.01$) and OH2-FLT3L ($p < 0.0001$) treatment groups suppressed tumor growth and extended the survival of mice compared with the control group. Furthermore, OH2-FLT3L treatment demonstrated superior tumor suppression ($p < 0.05$) and higher survival rates ($p < 0.05$) compared with OH2 treatment alone. Additionally, 42.9% (3 of 7) of mice in the OH2-FLT3L treatment group experienced complete tumor regression.

To verify that OH2-FLT3L can activate CTLs *in vivo*, splenic lymphocytes from treated mice were co-cultured with CT26 cells. Both

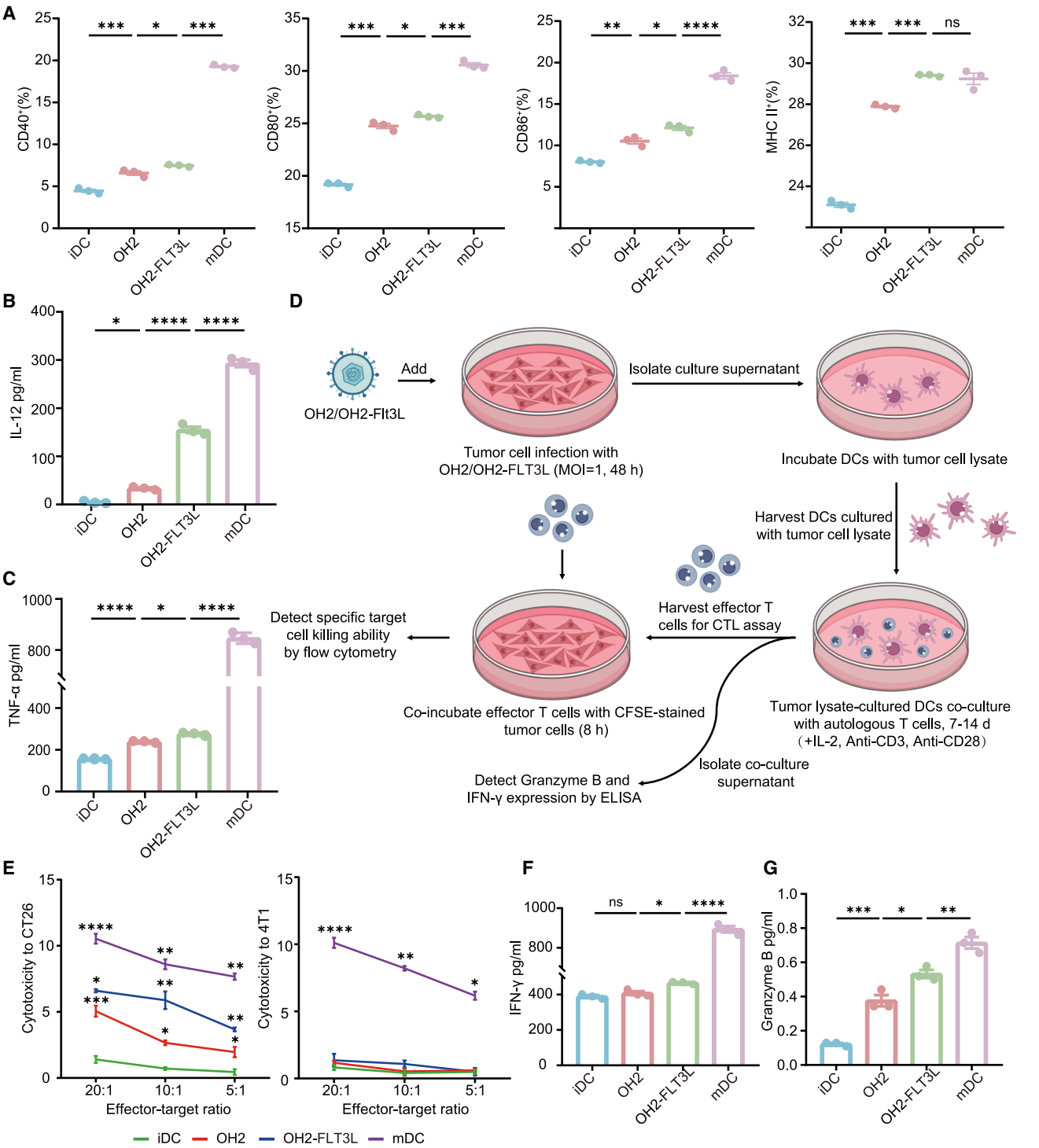

Figure 2. OH2-FLT3L induced DC activation and CTL immunity *in vitro*

Mouse BMDCs were prepared (iDCs, mDCs) and treated according to the specified protocol. As shown in Figure 2, iDCs and mDCs were used as controls. Following infection of CT26 cells with OH2/OH2-FLT3L (MOI = 1; 48 hpi), the supernatants were collected and co-cultured with iDCs (24 h). Flow cytometry (A) and ELISA (B and C) were utilized to assess activation/maturation phenotypes, viability, and the production of pro-inflammatory cytokines. (D) Schematic representation of the experimental design demonstrating that primary mouse DCs co-cultured with CT26 oncolytic materials stimulate a specific CTL immune response *in vitro*. (E–G) T cells co-cultured

(legend continued on next page)

OH2 and OH2-FLT3L treatment groups exhibited significant CTL activity, which correlated with the E:T ratio (Figures 3D and S4).

The rechallenge experiment demonstrated that all mice whose tumors completely regressed after the initial treatment showed no recurrence, while all mice from the control group experienced tumor recurrence 6 days after initial tumor inoculation (Figure 3E). These results suggested that OH2-FLT3L not only induced antitumor immunity *in vivo* but also effectively stimulated the generation of antitumor memory, preventing tumor recurrence.

We further validated the tumor growth suppression effects of OH2-FLT3L in the 4T1 mouse model (Figure 3F). Compared with the OH2 treatment group ($p = 0.0345$) and the control group ($p < 0.0001$), the OH2-FLT3L treatment group exhibited significantly enhanced tumor growth inhibition (Figure 3G). Additionally, mice in the OH2-FLT3L treatment group demonstrated significantly higher survival rates compared with the OH2 treatment group ($p = 0.0177$) and the control group ($p = 0.0009$) (Figure 3H). In the CTL cytotoxicity assay, T cells from mice in the OH2-FLT3L treatment group demonstrated significantly greater cytotoxicity against target cells at various E:T ratios (25:1, 50:1, 100:1) compared with those from the OH2 and control groups, consistent with the findings observed in the CT26 model (Figure 3I).

Subsequently, we performed immunohistochemical analysis on tumor tissues from mice (Figure 4A). The immunohistochemical results showed that the proportions of CD3+ T cells, CD4+ T cells, CD8+ T cells, and DC cells in the TME of mice treated with OH2 and OH2-FLT3L were significantly elevated (Figure 4B). Compared with mice treated with OH2, mice treated with OH2-FLT3L exhibited a significant increase in the infiltration of CD3+ T cells ($p = 0.0236$), CD4+ T cells ($p < 0.0001$), CD8+ T cells ($p < 0.0001$), and DC cells ($p < 0.01$) into the TME. Additionally, immune cells in the OH2-FLT3L treatment group were concentrated in the central region of the tumor, suggesting enhanced immune cell migration into the tumor core.

Furthermore, we performed flow cytometry analysis on the spleens of treated mice after treatment completion (Figures 4C–4J). Both OH2 and OH2-FLT3L treatments led to an increase in the proportions of CD3+ T cells (Figure 4C), CD4+ T cells (Figure 4D), CD8+ T cells (Figure 4E), and DC cells (Figure 4F), with OH2-FLT3L showing a more pronounced increase. Interestingly, in the CT26 model, both OH2 and OH2-FLT3L treatment groups showed a decrease in natural killer (NK) cell proportions (Figure 4G), while in the 4T1 model, there was no significant difference between the OH2 treatment and control groups ($p = 0.2777$). However, the proportion of NK cells in the spleens of the OH2-FLT3L group was significantly higher than that of the OH2 group ($p = 0.0005$) and the control group ($p = 0.0017$) (Figure S5). This may be because CT26 is typically considered a "hot tumor," where OH2 and OH2-FLT3L treatments activated T cells and DCs, causing T cells to dominate the antitumor immune response, while NK cells primarily respond to viral infections. Conversely, 4T1 tumors are generally considered "cold tumors," where NK cells may be more involved in tumor response. We also examined the changes in Gr-1+CD11b+ myeloid cells, which phenotypically align with murine myeloid-derived suppressor cells (MDSCs) (Figure 4H). Compared with the control group, both OH2 and OH2-FLT3L treatment groups showed a significant reduction in this population, with the OH2-FLT3L group exhibiting an even greater decrease ($p < 0.0001$). Additionally, after OH2 and OH2-FLT3L treatments, the proportion of CD44+ CD4+ and CD8+ T cells significantly increased (Figures 4I and 4J), with memory T cell increase being more pronounced in the OH2-FLT3L group compared with the OH2 group. This suggested that OH2-FLT3L treatment effectively activates T cells and may promote the formation of immunological memory, laying the foundation for long-term antitumor immunity.

OH2-FLT3L mobilizes distant immune responses in immunocompetent 4T1 and CT26 mouse models

We further explored whether OH2-FLT3L could induce both local and systemic immune responses targeting bilateral tumors. In the established bilateral CT26 tumor mouse model, only the right-side tumor was treated with five intratumoral injections. The results showed that the OH2 treatment group demonstrated tumor suppression on the injected side compared with the control group but failed to induce a systemic immune response against the distant tumor. In contrast, the OH2-FLT3L treatment group exhibited significant inhibition of both the injected and distant tumors, indicating a stronger ability to activate systemic immunity (Figures 5A and 5B). Similar results were observed in the bilateral 4T1 tumor mouse model, further validating the systemic antitumor effect of OH2-FLT3L (Figure 5C). In summary, OH2-FLT3L not only effectively suppressed the growth of the injected tumor but also induced a robust systemic immune response against distant tumors, demonstrating superior antitumor efficacy.

OH2-FLT3L in combination with anti-PD1 antibody enhances antitumor immune response in 4T1 and CT26 models

We have demonstrated that the novel virus OH2-FLT3L exhibits superior antitumor effects compared with its parental virus OH2. However, whether combining OH2-FLT3L with anti-PD1 antibody can reverse the immunosuppressive TME and convert "cold tumors" to "hot tumors," thereby enhancing the antitumor efficacy of ICIs, requires further investigation. Therefore, we established a subcutaneous CT26 model in BALB/c mice (Figure 5D). One week after tumor

with iDCs, mDCs, and OH2/OH2-FLT3L-induced DCs were co-cultured with syngeneic CT26 or irrelevant 4T1 cells for 8 h at the indicated ratios. Flow cytometry (E) was used to assess cytotoxicity, and ELISA was employed to measure the levels of IFN-γ (F) and Granzyme B (G) secreted by T cells. $n = 3$ samples per group, with error bars representing the SEM; statistical analysis was conducted using multiple comparisons ANOVA. ns indicates no significant differences; $^{*}p < 0.05$; $^{**}p < 0.01$; $^{***}p < 0.001$; $^{****}p < 0.0001$.

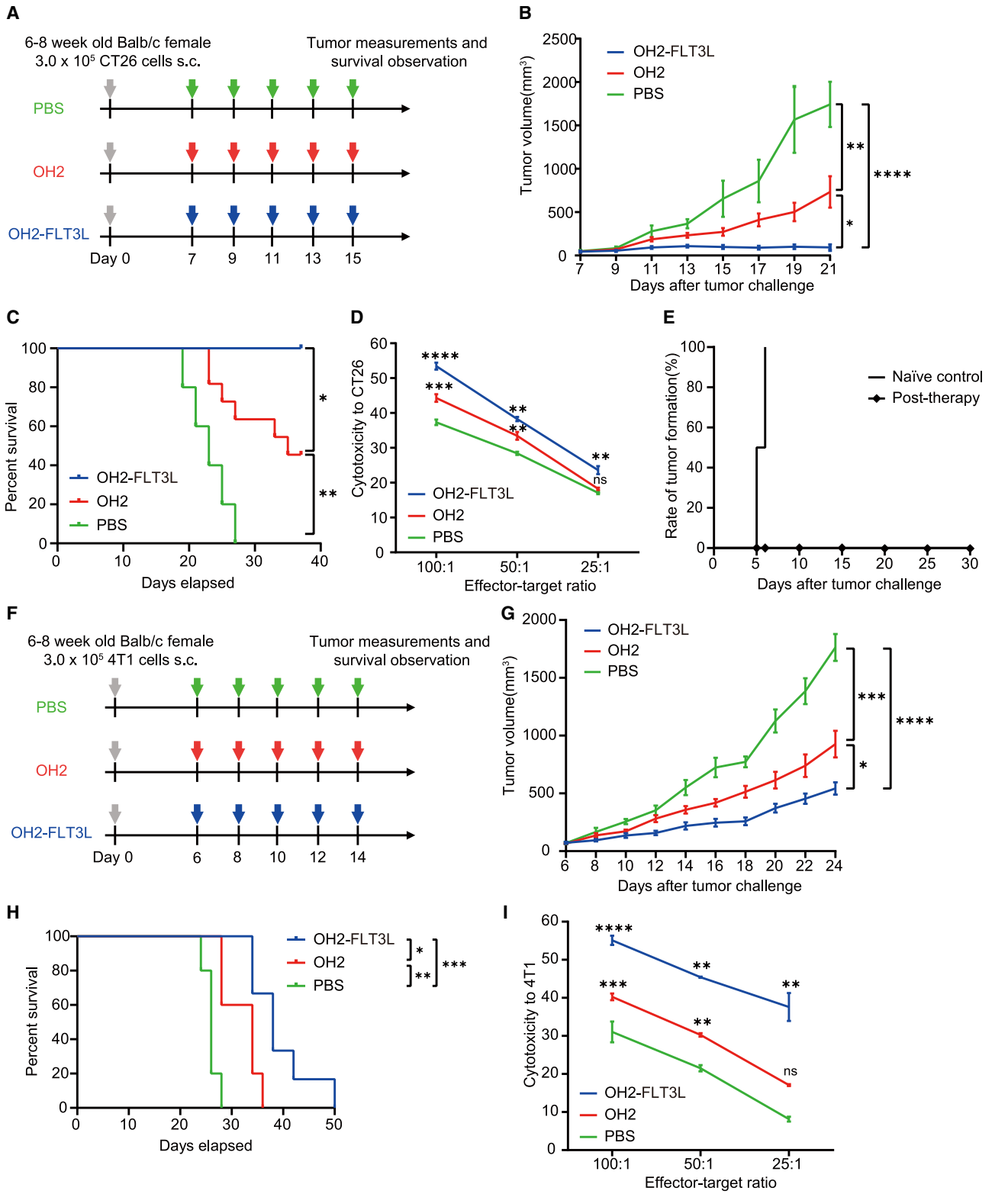

(legend on next page)

inoculation, the mice were divided into five treatment groups: PBS control, OH2 treatment, anti-PD1 treatment, OH2-FLT3L treatment, and OH2-FLT3L combined with anti-PD1 antibody (n = 5 per group). The results showed that both anti-PD1 antibody alone ($p < 0.0001$) and OH2 treatment alone ($p = 0.0009$) significantly reduced tumor burden compared with the control group (Figure 5E). However, the tumor growth inhibition by OH2-FLT3L was not significantly enhanced compared with the anti-PD1 antibody treatment group ($p = 0.2644$). In contrast, the combination of OH2-FLT3L and anti-PD1 antibody significantly enhanced tumor growth inhibition compared with either anti-PD1 alone ($p = 0.0065$) or OH2 alone ($p = 0.0001$). Moreover, compared with the control group, both anti-PD1 antibody treatment ($p = 0.0021$) and OH2 treatment ($p = 0.0127$) significantly improved survival, while OH2-FLT3L ($p = 0.0021$) and the combination treatment group ($p = 0.0021$) showed the most pronounced therapeutic response (Figure 5F).

Similar results were obtained in the 4T1 model (Figure 5G), where both OH2-FLT3L monotherapy and combination therapy showed significant tumor growth inhibition (Figure 5H) and extended survival (Figure 5I) compared with anti-PD1 alone.

In summary, these results demonstrated that the combination of OH2-FLT3L and anti-PD1 antibody not only effectively suppressed tumor growth but also significantly prolonged mouse survival, indicating that this combination therapy significantly enhanced tumor growth suppression.

OH2-FLT3L enhances TME modulation through immune cell interactions and signaling pathway activation

We used single-cell sequencing to characterize the tumor microenvironment (TME) in greater detail. Single-cell data showed that immune cells within the TME could be divided into CD4+ T cells, CD8+ T cells, NK cells, mast cells, myeloid cells, neutrophils, and B-plasma cells (Figure 6A). The proportions of each immune cell subset are shown in Figure 6B. Compared with the control group, the OH2-FLT3L group showed a significant increase in CD4+ T cells, NK cells, and neutrophils, while myeloid cells were significantly decreased (Figure S6). Analysis of T cell subsets (Figures 6C, 6D, and S7) revealed a significant reduction in exhausted CD8+ T cells (Tex CD8+T) and naive CD8+ T cells in the OH2-FLT3L group compared with the OH2 group. Interaction analysis of T and NK cells across treatment groups (Figures 6E–6J) showed that after OH2 treatment, the signaling received by cycling CD8+ T cells from various NK subsets was reduced, and inter-signaling among NK subsets was also weakened. After OH2-FLT3L treatment, cycling CD8+ T cells exhibited reduced signaling from NK_Sell (NK cells expressing high levels of Sell, associated with a more naive or migratory phenotype) and NK_Gzmg (NK cells expressing high levels of granzyme G, indicative of cytotoxic activity), while inter-signaling among NK subsets was enhanced. Additionally, interactions between cycling CD8+ T cells, Tex CD8+ T cells, and Tex-Ccr7 CD8+ T cells with NK cells were strengthened. After both OH2 and OH2-FLT3L treatments, interactions among cycling CD8+ T cells, Tex CD8+ T cells, and Tex-Ccr7 CD8+ T cells were enhanced. It suggested that oncolytic virus therapy can effectively reshape the tumor immune microenvironment. More importantly, OH2-FLT3L could further activate the antitumor immune response and reduce the exhausted T cells in the tumor microenvironment, thus achieving better antitumor effects.

The cell interaction analysis of pathways between T and NK cells (Figures 7A and 7B) revealed that the OX40 signaling pathway was present exclusively in the OH2-FLT3L group, where NK_Gzmg cells transmit signals to other T cells. The OX40 pathway mediated interactions between NK cells and T cells as well as other immune cells, thereby enhancing the antitumor immune response. Additionally, the FASLG signaling pathway was also observed only in the OH2-FLT3L group (Figures 7C and 7D), with CD4+ Treg cells receiving signals from other CD8+ T and NK cells.

DISCUSSION

Here, we designed a novel OV, OH2-FLT3L, and demonstrated its ability to induce systemic tumor regression by activating DCs and antigen-specific cytotoxic T cells in both *in vitro* and *in vivo* models. Our findings showed that OH2 armed with FLT3L increases the proportion of activated DCs in the spleen and TME, leading to CTL-mediated antitumor immunity and the regression of distant tumors. We observed that OH2-FLT3L also modulates the proportions of NK cells, Gr-1+CD11b+ myeloid cells, and memory T cells, effectively enhancing antitumor therapy by strengthening the DC/T cell axis. Furthermore, OH2-FLT3L induced long-term memory in mice bearing CT26 tumors and showed effective modulation of the TME in mice bearing 4T1 tumors, triggering tumor-specific immune responses. Additionally, single-cell transcriptomics analysis further elucidated the regulatory effects of OH2-FLT3L treatment on

Figure 3. OH2-FLT3L treatment inhibited tumor growth and generated antigen-specific antitumor immunity

(A) Schematic representation of the experimental design for the CT26 model. (B) Tumor growth curves of mice in different treatment groups of the CT26 model. PBS group, $n = 5$; OH2 group, $n = 11$; OH2-FLT3L group, $n = 7$. (C) Kaplan-Meier survival curves of mice in different treatment groups of the CT26 model were analyzed using the log rank test. (D) Following the completion of treatment, mice were euthanized, and splenic lymphocytes were isolated and co-cultured with CT26 cells at specified ratios for 6–8 h. Cells were then collected for cytotoxicity assessment using flow cytometry. (E) Seven mice with complete tumor regression after initial treatment underwent a second tumor challenge by subcutaneously inoculating 3×10^5 CT26 cells into the contralateral dorsal side. Additionally, eight untreated BALB/c mice were inoculated with the same dose of CT26 cells as controls to observe tumor incidence. (F) Schematic representation of the experimental design for the 4T1 model. (G) Tumor growth curves of mice in different treatment groups of the 4T1 model. PBS group, $n = 5$; OH2 group, $n = 7$; OH2-FLT3L group, $n = 6$. (H) Kaplan-Meier survival curves of mice in different treatment groups of the 4T1 model were analyzed using the log rank test. (I) Following the completion of treatment, mice were euthanized, and splenic lymphocytes were isolated and co-cultured with 4T1 cells at specified ratios for 6–8 h. Cells were then collected for cytotoxicity assessment using flow cytometry. Error bars represent the SEM, and statistical analysis was conducted using multiple comparisons ANOVA. ns indicates no significant differences; $^*p < 0.05$; $^{**}p < 0.01$; $^{***}p < 0.001$; $^{****}p < 0.0001$.

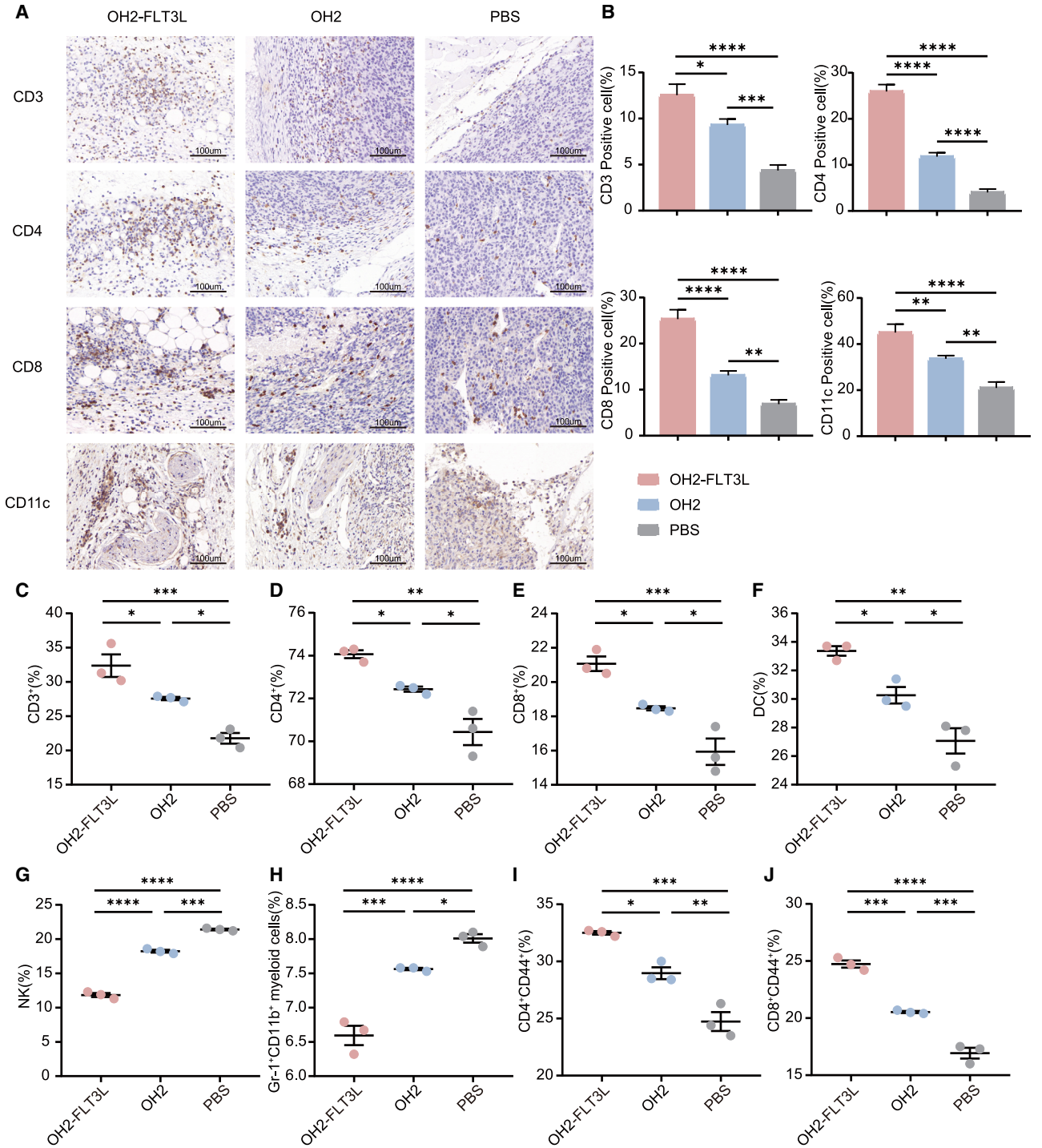

Figure 4. OH2-FLT3L induced tumor dendritic cell and T cell infiltration, stimulating an increase in the proportion of immune effector cells in the spleen

(A) Representative IHC staining results for CD3, CD4, CD8, and CD11c in the OH2-FLT3L treatment group, OH2 treatment group, and PBS control group. Scale bar, 100 μm; $n = 5$ samples per group. (B) Positive cell rates for CD3, CD4, CD8, and CD11c in the OH2-FLT3L treatment group, OH2 treatment group, and PBS control group. $n = 5$ samples per group; proportions represent the percentage of cells relative to the total cell count. (C–J) After treatment completion, splenic lymphocytes were isolated from mice and prepared as single-cell suspensions for flow cytometry analysis of T cell subtypes (C–E), DCs (defined as Gr-1-MHC II + CD11c+CD11b+) (F), NK

(legend continued on next page)

signaling pathways between immune cells. We found that after OH2-FLT3L treatment, signaling between NK cell subsets increased, while interactions between cycling CD8+ T cells and NK cells decreased. Moreover, activation of the OX40 and FASLG pathways was observed exclusively in the OH2-FLT3L group, where OX40 promotes T cell activation and proliferation,[22] while FASLG signaling influences Treg proliferation and function. These findings indicate that OH2-FLT3L effectively enhances antitumor responses within the immune microenvironment by activating specific pathways and strengthening intercellular signaling.

OVs are considered a novel therapeutic approach for cancer, capable of selectively replicating within tumor cells and inducing ICD, with toxicity profiles that generally do not overlap with other cancer treatments.[19,23] To date, four OVs have been approved for clinical cancer therapy, although T-VEC remains the only therapy widely approved.[24] Similar to T-VEC, our OH2-FLT3L is constructed from an attenuated OH2 virus, with deletions of ICP47 and ICP34.5. These modifications reduce the potential pathogenicity of OH2 while enhancing its therapeutic safety. In a recent phase I/II clinical trial, the OH2 used in this study demonstrated good tolerability and durable antitumor activity in patients with advanced solid tumors, particularly those with metastatic esophageal and rectal cancers.[25] Another phase I clinical trial combining OH2 with anti-PD-L1 antibody for colorectal cancer (CRC) showed a 35.9% tumor response rate, with partial responders achieving a progression-free survival of 313 days.[26] These results demonstrate that OH2 is a promising OV therapeutic strategy, and its combination with other immunotherapies can elicit stronger antitumor immune responses.

Although many previous studies have explored the clinical benefits of OVs in cancer therapy, they have mainly focused on adaptive immunity. Enhancing the antitumor functions of innate immune cells such as DCs and combining them with OVs remains an emerging strategy. The initiation and persistence of antitumor immunity depend on the presentation of tumor antigens to naive T cells. However, the low infiltration of effector immune cells in immune-evasive TMEs, or "cold tumors," significantly hinders this process.[27–29] FLT3L, a transmembrane/soluble cytokine critical for B cell and dendritic cell (DC) development,[12,30–32] drives the differentiation of DC progenitor cells (CDPs) into conventional DC subsets (cDC1s and cDC2s) through FLT3 receptor signaling.[33,34] This process expands DC abundance and enhances their functional maturation within the tumor microenvironment (TME), thereby amplifying antigen presentation and subsequent T cell-mediated antitumor immunity. Earlier studies have demonstrated that FLT3L administration promotes DC proliferation and activation, correlating with improved tumor control in animal models.[35–38]

Many studies have explored the combination of replication-defective vectors, such as adenoviruses, with FLT3L for cancer therapy.[39] Bernt et al. showed that adenoviral vectors expressing FLT3L could compensate for the inability of FLT3L to induce DC maturation.[40] In brain glioma models, Ali et al. demonstrated that engineered adenoviruses expressing FLT3L increased DC infiltration in CNS-1 tumors in rats.[41] A Phase 1 clinical trial demonstrated the safety and efficacy of adenoviral vectors expressing FLT3L in the treatment of adult high-grade gliomas.[42] Other studies have further confirmed that intratumoral (i.t.) injection of FLT3L not only activates and expands DCs but also recruits them to the TME and TDLNs,[14,43] similar to the results observed in our study.

Oncolytic viruses, in contrast to replication-defective vectors, have stronger replication capacities, allowing them to spread more widely within tumor tissues and effectively infect more tumor cells. Barnard et al. showed that treatment with G47Δ, an oncolytic virus expressing FLT3L, increased survival rates in glioma-bearing mice.[44] Similarly, in our study, the OH2-FLT3L virus demonstrated a marked improvement in tumor control and immune response activation in the 4T1 mouse model. Compared with the CT26 model, both OH2-FLT3L alone and in combination with anti-PD1 antibody showed significant tumor growth inhibition and prolonged survival in the 4T1 model compared with anti-PD1 antibody alone. This could be because 4T1 tumors, which are poorly infiltrated by immune cells and considered "cold tumors," typically respond poorly to ICIs alone. However, OH2-FLT3L may improve the TME by recruiting DCs and T cells. These results indicate that OH2-FLT3L enhances DC recruitment and function, showing great potential in overcoming the immunosuppressive TME of cold tumors and providing strong support for further optimization of CIT, particularly in combination with ICIs.

Based on the aforementioned effect of OH2-FLT3L on DC recruitment, we further investigated its specific effects on DC maturation *in vitro*. Our *in vitro* DC induction experiments showed that the surface costimulatory molecules CD40, CD80, CD86, and MHC II were significantly upregulated on DCs treated with OH2-FLT3L oncolysates. CD40 is an important immunological mediator linking innate and adaptive immunity, promoting the production of cytokines and chemokines by DCs, inducing the expression of costimulatory molecules, and facilitating antigen presentation to T cells.[45,46] CD80 and CD86 provide necessary costimulatory signals that promote T cell survival and proliferation,[47] while MHC II molecules are critical for presenting processed tumor antigens to CD4+ T helper cells.[8] Furthermore, our study observed a significant increase in IL-12 and TNF-α secretion by OH2-FLT3L-induced DCs. Concurrently, OH2-FLT3L-induced CTLs exhibited a marked elevation in IFN-γ secretion, which may activate cDCs to secrete more IL-12, further

cells (defined as CD3-CD49b+) (G), Gr-1+CD11b+ myeloid cells (defined as Gr-1+CD11b+) (H), and memory T cells (defined as CD4+CD44+ or CD8+CD44+) (I and J). Data are presented as individual independent replicates. Error bars represent the SEM, and statistical analysis was conducted using multiple comparisons ANOVA. ns indicates no significant differences; $^{*}p < 0.05$; $^{**}p < 0.01$; $^{***}p < 0.001$; $^{****}p < 0.0001$. Collectively, these results suggested that OH2-FLT3L effectively inhibited tumor growth, enhanced antitumor immune responses, and promoted the formation of immune memory *in vivo*.

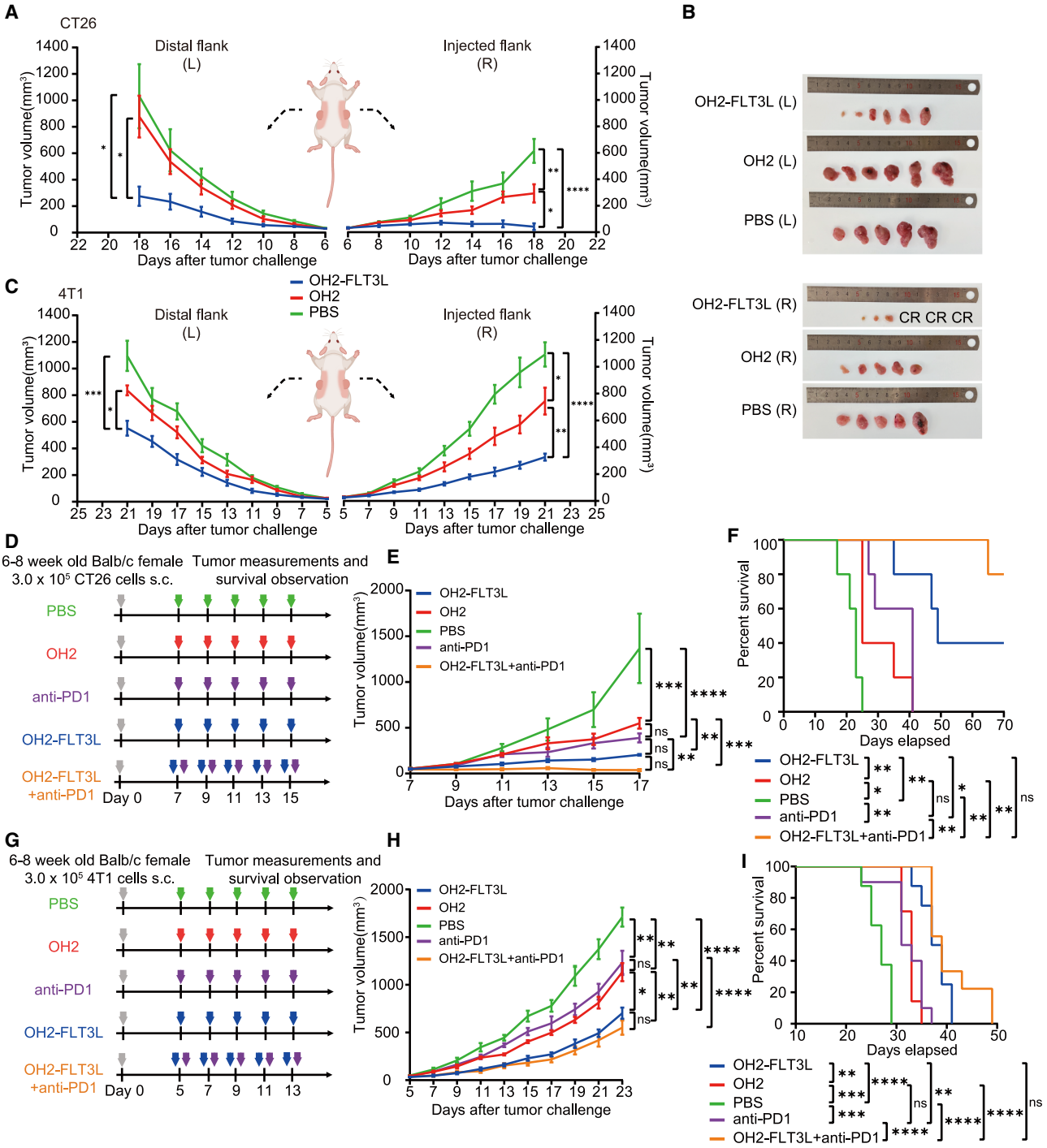

Figure 5. OH2-FLT3L induced systemic immune responses in the 4T1 and CT26 models, and its combination with anti-PD-1 antibody further enhanced antitumor immune responses

(A–C) Five- to 8-week-old BALB/c mice were injected bilaterally with 3 × 10^5 CT26 or 4T1 cells, and on the sixth day post-tumor implantation, PBS, OH2, or OH2-FLT3L was administered only at the right-side tumor site. (A) Tumor growth curves of mice in different treatment groups of the CT26 model, n = 5–6 mice per group. (B) Photos of tumors harvested from mice in all groups of the CT26 model on day 18 after tumor inoculation. CR: complete response. (C)Tumor growth curves of mice in different treatment groups of the 4T1 model, n = 8 mice per group. (D) Schematic representation of the combined treatment experimental design for the CT26 model. (E) Tumor growth curves of mice in different treatment groups of the CT26 model, n = 5 mice per group. (F) Kaplan-Meier survival curves of mice in different treatment groups of the CT26 model were analyzed

(legend continued on next page)

stimulating CD8+ T cells, enhancing DC-T cell crosstalk,[48] thereby inducing a stronger antitumor immune response compared with OH2. This aligns with previous findings showing that cDC1-mediated presentation induces a stronger immune response by CD8+ CTLs.[49]

Our study, however, has certain limitations. While OH2-FLT3L has demonstrated its capacity to remodel the TME through DC activation, the precise mechanisms, such as how FLT3L affects various DC subsets and their roles within the TME, require further investigation. Moreover, the optimal combinations and administration regimens for using OH2-FLT3L with other immunotherapies need to be systematically studied to fine-tune dosage and frequency. Finally, the abundance of DC subsets and the tumor type-specific differences in patients could impact the efficacy and clinical outcomes of OH2-FLT3L. Variability in tumor type or heterogeneity may influence patient responses to viral infection and immunotherapy, highlighting the need for further studies on tailoring OH2-FLT3L's clinical application strategies to these differences.

The safety and tolerability of OH2 have been confirmed in clinical trials, and the new virus OH2-FLT3L did not exhibit significant toxicity in mouse models, laying the groundwork for its clinical application. Although our murine model employed an every-other-day dosing regimen to counteract the rapid progression of tumors, inherent differences in pharmacokinetics and pharmacodynamics between mice and human patients suggest that a longer dosing interval may be necessary for clinical translation—consistent with the phase I/II trial design of our parental OH2, which involves dosing every 2 weeks.[25] Our preclinical model serves to validate the enhanced immune effects of FLT3L within the OH2 platform, while the clinical safety data of the parental virus provide further assurance for human application. Future clinical optimization could explore an intermediate dosing frequency to ensure safety while effectively managing high tumor burdens in patients.

Additionally, the production process for engineered OVs is relatively mature, enabling large-scale cultivation and reducing production costs, thus promoting the accessibility of CIT. OH2-FLT3L can reshape the TME by activating DCs, enhancing tumor-specific immune responses, and demonstrating superior tumor inhibition in mouse models. Additionally, the remarkable efficacy of OH2-FLT3L in combination with anti-PD-1 suggests potential synergies with other immunotherapeutic approaches, such as Toll-like receptor agonists, which could further enhance DC maturation and activation. Alternatively, adoptive cell therapy (ACT) could be combined, where DC activation enhances antigen presentation, improving T cell recognition and cytotoxicity against tumors.

In summary, our data support the feasibility of OH2-FLT3L as a novel oncolytic viral therapy. The introduction of FLT3L enhances the efficacy of CIT by promoting the cross-presentation of tumor antigens from DCs to T cells.

MATERIALS AND METHODS

Cell lines

The cell lines used in this study included Vero (African green monkey kidney cells), CT26 (murine colon cancer cells), B16R (murine melanoma cells), and 4T1 (murine breast cancer cells). Vero cells were obtained from ATCC and maintained in our laboratory. The 4T1 and CT26 cells were purchased from the National Infrastructure of Cell Line Resource (Beijing, China). B16R was constructed in our laboratory by stably transfecting parental B16F10 cells with HSV receptors.[50] CT26 and 4T1 were cultured in RPMI-1640 medium (Gibco) supplemented with 10% fetal bovine serum (FBS). All cell lines were grown at 37°C in a 5% CO_2 incubator.

Oncolytic virus

OH2 was provided by Binhui Biopharmaceutical Co., Ltd. (Wuhan, China). It is an attenuated OV derived from the wild-type HSV-2 strain HG52, with deletions of the ICP47 and ICP34.5 genes.[21,51]

OH2-FLT3L was engineered from OH2. First, using a previously constructed pHG52d34.5-CMV-eGFP plasmid,[52] we generated the pHG52d34.5-CMV-FLT3L plasmid following the same methodology. Vero cells were cultured, infected with the OH2-eGFP virus, and the viral genome was extracted. The pHG52d34.5-CMV-FLT3L plasmid, OH2-eGFP viral genome, and sg GFP-gRNA-Cas9 were co-transfected into Vero cells, facilitating the replacement of the eGFP gene with FLT3L through CRISPR-Cas9 homologous recombination, resulting in the OH2-FLT3L recombinant virus. The recombinant OH2-FLT3L virus was purified following 5–8 rounds of plaque assays under fluorescence microscopy. The construct was validated via sequencing, expanded in Vero cells, titrated, aliquoted, and stored at −80°C until use. The modified region of the viral structure was confirmed by PCR followed by agarose gel electrophoresis (Figures S1A and S1B) and sequencing (Figure S1C).

Mice

Female BALB/c mice, aged 6–8 weeks, were purchased from Beijing Vital River Laboratory Animal Technology Co., Ltd. All animals were housed under specific pathogen-free (SPF) conditions in individually ventilated cages (IVC). Some of the animal experiments were conducted at Beijing Keweite Animal Technology Co., Ltd. All animal-related procedures were approved by the Animal Experiment Ethics Committee of the National Cancer Center/Cancer

using the log rank test. (G) Schematic representation of the combined treatment experimental design for the 4T1 model. (H) Tumor growth curves of mice in different treatment groups of the 4T1 model. PBS group, $n = 8$; OH2 group, $n = 7$; OH2-FLT3L group, $n = 8$; anti-PD1 group, $n = 10$; OH2-FLT3L + anti-PD1 group, $n = 9$. (I) Kaplan-Meier survival curves of mice in different treatment groups of the 4T1 model were analyzed using the log rank test. Error bars represent the SEM, and statistical analysis was conducted using multiple comparisons ANOVA. ns indicates no significant differences; $^{*}p < 0.05$; $^{**}p < 0.01$; $^{***}p < 0.001$; $^{****}p < 0.0001$.

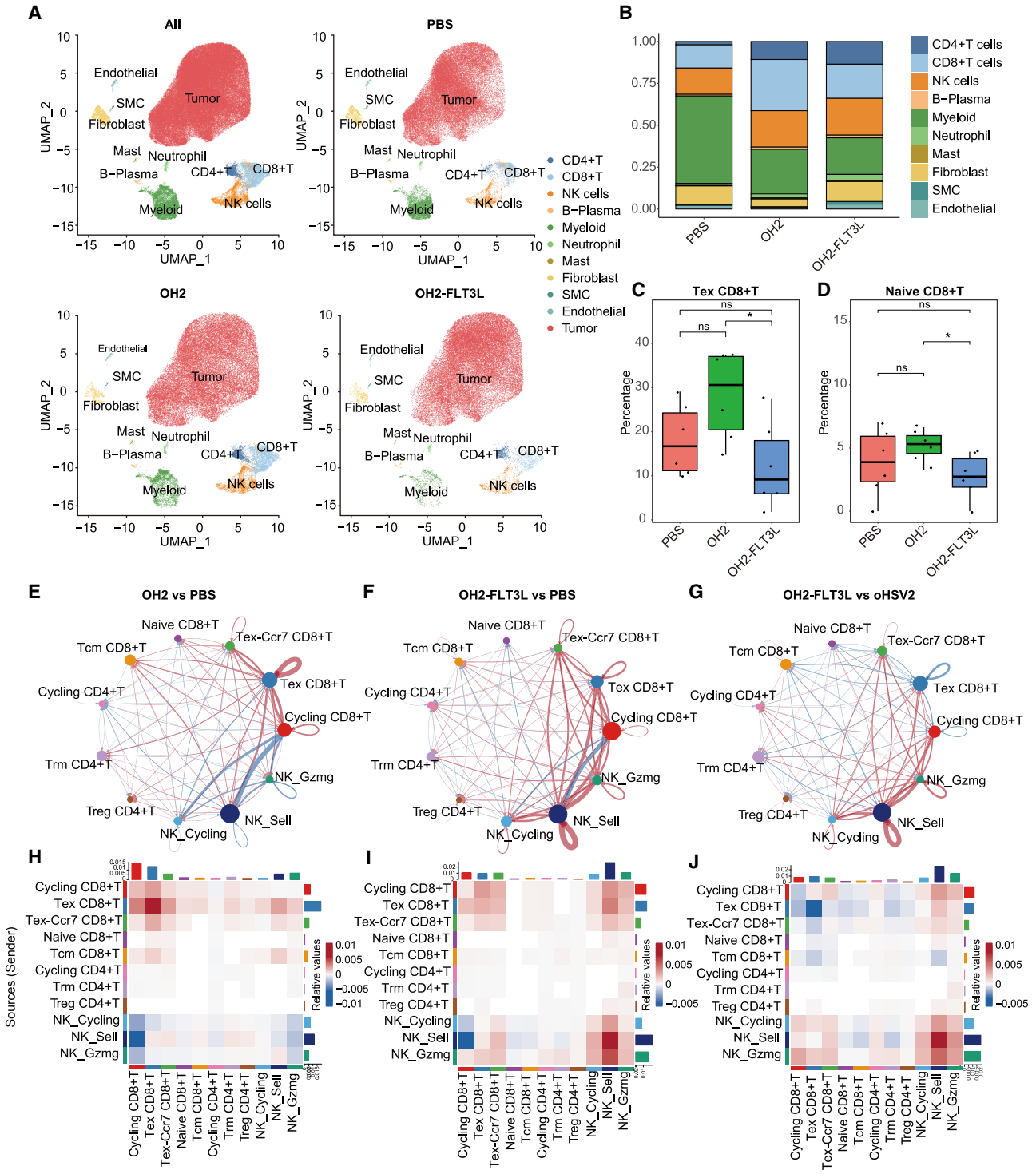

Figure 6. Single-cell sequencing revealed the tumor immune microenvironment in tumor tissues from different treatment groups

(A) Clustering of various cell types across single-cell data in the overall dataset and in each treatment group. SMC: smooth muscle cell. (B) Proportions of different immune cell subsets in the single-cell data. (C and D) Proportions of Tex CD8+T cells and naive CD8+ T cells in each treatment group. (E–G) Network diagrams showing differences in

(legend continued on next page)

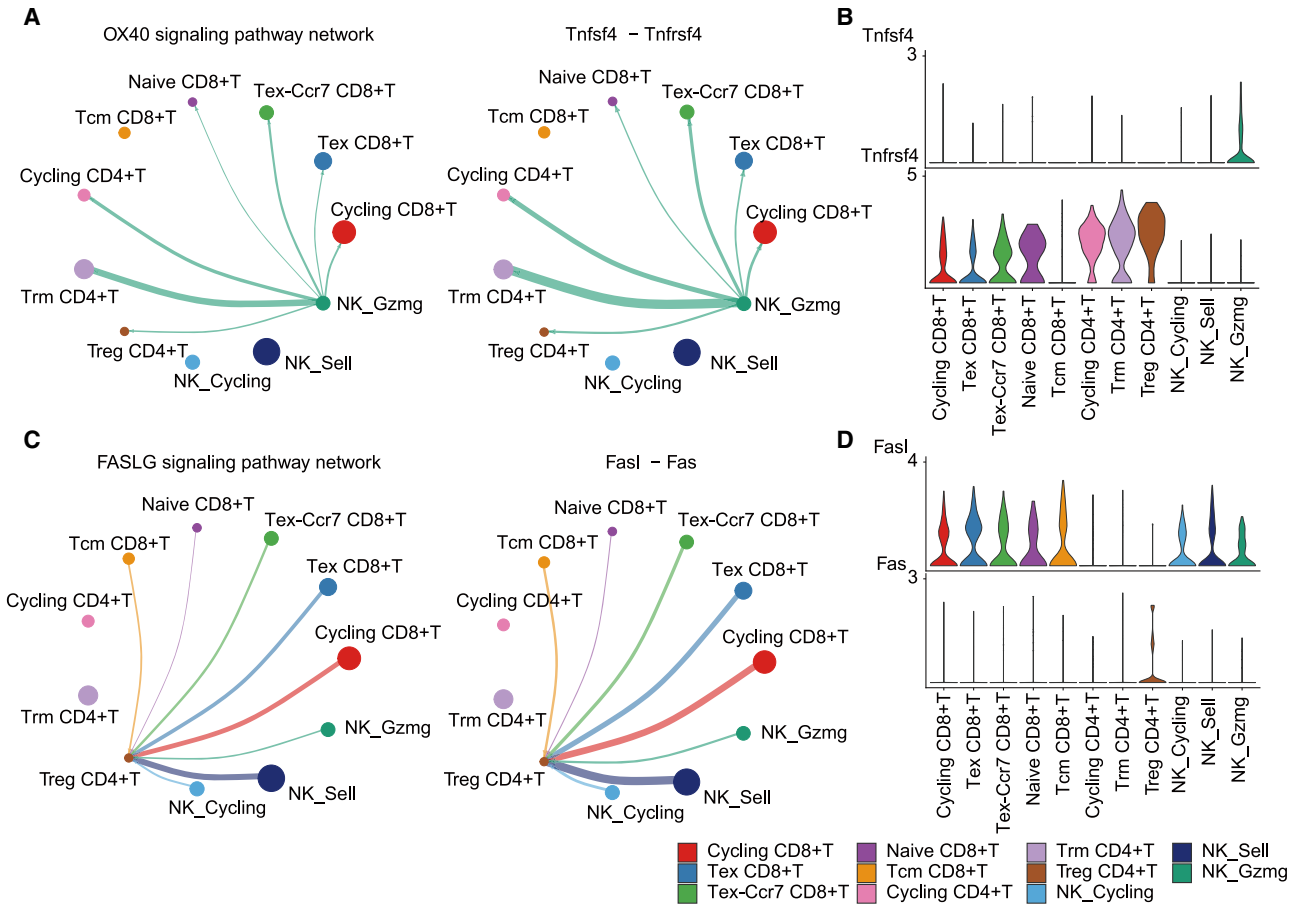

Figure 7. OH2-FLT3L induced T and NK cell interactions mediated by OX40 and FASLG signaling pathways

(A) Network diagram of cell interactions via the OX40 signaling pathway and its ligand-receptor pair, Tnfsf4-Tnfrsf4. (B) Violin plots showing expression levels of Tnfsf4 and Tnfrsf4 in different T cell and NK cell subsets within the OH2-FLT3L treatment group. (C) Network diagram of cell interactions via the FASLG signaling pathway and its ligand-receptor pair, FasI-Fas. (D) Violin plots showing expression levels of FasI and Fas in different T cell and NK cell subsets within the OH2-FLT3L treatment group.

Hospital, Chinese Academy of Medical Sciences and Peking Union Medical College (No. NCC2021A282).

CCK8 cell viability assay

The cell viability was assessed using a CCK8 assay (Cell Counting Kit-8, DOJINDO, Japan). Cells were seeded in 96-well plates at densities ranging from 5×10^3 to 1×10^4 cells per well, with each condition tested in triplicate. Twenty-four hours later, the cells were infected with either OH2 or OH2-FLT3L at MOIs of 0.1, 1, and 5 to assess the impact of MOI on cell viability. At 24, 48, and 72 h post-infection, the culture medium was removed, and 100 μL of a mixture containing 10% CCK8 reagent was added to each well. The plates were then incubated for an additional 2 h. Finally, cell viability was quantified using the iMark Microplate Absorbance Reader (Bio-Rad, Japan) at a wavelength of 450 nm.

FLT3L expression confirmation

Logarithmically growing 4T1, CT26, and Vero cells were seeded into six-well plates. When cells reached 70%–80% confluence, they were washed with PBS and then incubated with 1 mL of serum-free RPMI-1640 medium. The cells were subsequently infected with either OH2 or OH2-FLT3L at MOIs = 0.1, 1, and 5. After 1 h, the cells were replenished with 1 mL of RPMI-1640 medium containing 10% FBS. Culture supernatants were collected at 24, 48, and 72 h post-infection. The supernatants were centrifuged at 400 × *g* for 5 min at 4°C to remove any cell debris and then stored at −80°C until further

interaction strength between T and NK cells among treatment groups. Tcm CD8+T: central memory CD8+ T cells; Trm CD4+ T: tissue-resident memory CD4+ T cells; Treg CD4+T: regulatory CD4+ T cells. (H–J) Heatmaps illustrate differences in interaction intensity between T and NK cells across treatment groups. $n = 3$ mice per group, with each biological sample generating two independent FASTQ files. Statistical significance was determined using an independent samples t test. ns indicates no significant differences; $^*p < 0.05$; $^{**}p < 0.01$; $^{***}p < 0.001$; $^{****}p < 0.0001$.

analysis. Flt3L levels in the culture supernatants were quantified using a Mouse FMS-like Tyrosine Kinase 3 Ligand ELISA Kit (Jingmei Biotechnology) following the manufacturer's protocol.

Silver staining and western blotting

Logarithmically growing CT26 cells were passaged into 10 cm^2 culture dishes. When the cells reached 70%–80% confluence, they were washed with PBS, followed by the addition of 8 mL of serum-free RPMI-1640 medium. The cells were then infected with OH2 or OH2-FLT3L (MOI = 1). At 8 h, 24 h, and 48 h post-infection, the supernatant proteins were collected by centrifugation at 4500 rpm for 15 min at 4°C using Millipore Amicon Ultra filters (10 kDa MWCO). Protein concentrates were retrieved on ice. The cell pellet proteins were obtained by directly adding the mixture of RIPA and cocktail. SDS-PAGE was performed using 10% and 12.5% gels from the PAGE Gel Fast Preparation Kit (Epizyme, PG212, PG213). Silver staining was performed with the Fast Silver Stain Kit (Beyotime Biotechnology, P0017S). Western blot analysis was conducted using the following antibodies: HSP70 Rabbit mAb 8196 (Nature Biosciences, A15575) at a dilution of 1:1,000, HSPA14 Rabbit mAb [OJG2] (Nature Biosciences, A72794) at a dilution of 1:1,000, HMGB1 (D3E5) Rabbit mAb (Cell Signaling Technology #6893) at a dilution of 1:1,000, Beta Actin Rabbit mAb [SLMD] (Nature Biosciences, RA0001) at a dilution of 1:5,000, and Sodium Potassium ATPase Rabbit mAb [GJ8D] (Nature Biosciences, A54551) at a dilution of 1:1,000.

Preparation of oncolysate

Logarithmically growing CT26 cells were passaged into 10 cm^2 culture dishes. Once cells reached 70%–80% confluence, they were washed with PBS, and 4 mL of serum-free RPMI-1640 medium was added. Cells were then infected with OH2 or OH2-FLT3L (MOI = 1). After 1 h, 4 mL of RPMI-1640 medium containing 10% FBS was added. At 48 hpi, the supernatant was collected, centrifuged at 400 × *g* for 5 min at 4°C, and stored at −80°C for future use.

BMDC isolation

BMDCs were isolated from the femurs and tibias of 6- to 8-week-old mice using a modified Inaba method.[53] BMDCs were cultured in RPMI-1640 medium containing 10% FBS, supplemented with granulocyte-macrophage colony-stimulating factor (GM-CSF) (25 ng/mL) and IL-4 (10 ng/mL). On day 6, iDCs were harvested. Throughout DC handling, GM-CSF and IL-4 concentrations remained constant. On day 7, 1 mL of the prepared oncolysate was added to 1×10^6 iDCs for 24 h to obtain OH2 or OH2-FLT3L oncolysate-induced DCs. To generate mDCs, LPS (1 μg/mL) was added to the iDC culture medium for 24 h. On day 8, BMDCs were collected from the culture suspension for subsequent flow cytometry and ELISA analyses (Mouse IL-12 p70 ELISA Kit, abs520006-96T, Absin; Mouse TNF-α ELISA Kit(Plus), abs552204-96T, Absin).

Flow cytometric analysis of DC activation phenotypes

After collecting iDCs, mDCs, and OH2 or OH2-FLT3L oncolysate-induced DCs, cells were divided into multiple staining panels. They were incubated in the dark on ice with antibodies: CD11c (FITC, 117306; BioLegend), CD40 (APC, 124612; BioLegend), CD80 (APC, 104714; BioLegend), CD86 (APC, 159216; BioLegend), and I-A/I-E (APC, 107614; BioLegend). Flow cytometry was performed using a BD-LSRII system, and results were analyzed with FlowJo software.

In vitro study on OH2-FLT3L oncolysate stimulating DC-driven T cells

iDCs, mDCs, and OH2 or OH2-FLT3L oncolysate-induced DCs were obtained following the previously described steps. On day 8 of DC culture, lymphocytes were isolated from mouse spleens using lymphocyte separation liquid (DKW33-R0100, Shenzhen Dakewei Biotechnology Co., Ltd). The ratio of DCs to splenic T cells was adjusted to 1:10. Both DCs and T cells were seeded in 24-well plates pre-coated with 5 μg/mL Anti-Mouse CD3 SAFIRE Purified (Biogems, 05112-25) and Anti-Mouse CD28 SAFIRE Purified (Biogems,10312-20), which provided essential survival and proliferation signals for T cells. CTL stimulation medium was added (RPMI1640 with 10% FCS, 2 mM L-glutamine, 20 mM HEPES, 1 mM sodium pyruvate, 0.1 mM MEM non-essential amino acids, 100 IU/mL penicillin, 100 IU/mL streptomycin, and 5×10^{-5} M β-mercaptoethanol), maintaining T cell density at 2×10^6 cells/mL. On day 3, 100 U/mL IL-2 was added, and every 4–5 days, an additional 50 U/mL was supplemented. On days 12–14, T cells were harvested, counted, and used as effector cells in CTL assays.

CTL assay

Tumor cells were used as target cells, labeled with 0.5 mM CFSE at 37°C for 8 min. After labeling, cells were collected and adjusted to 4×10^5/mL. Then, T cells (effectors) and tumor cells (targets) were mixed at E:T ratios of 20:1, 10:1, and 5:1 (for *in vivo* experiments, 100:1, 50:1, and 25:1) and plated onto untreated U-bottom 96-well plates (Corning, 3795). After incubation at 37°C with 5% CO_2 for 4–6 h, cells were collected and stained with 2.5 μg/mL PI for 5 min at room temperature, followed by flow cytometry analysis. Cytokine expression in the co-culture supernatant was assessed via ELISA (Mouse IFN-γ ELISA Kit, MultiSciences; Mouse Granzyme B ELISA Kit, MultiSciences).

Animal model construction

Single-lesion animal model

Tumor cell lines (3×10^5) were injected subcutaneously into the right dorsal region of the mice. When tumor diameters reached 3–5 mm (approximately 5–7 days), mice were divided into three groups (OH2-FLT3L, OH2, and control groups), with n = 5–11 mice per group. The treatment protocol was as follows: (1) OH2 or OH2-FLT3L (2×10^6 pfu) was injected i.t. every other day for a total of five injections; (2) PBS (100 μL) was used as a control, injected i.t. every other day for a total of five injections. Tumor diameter, mouse body weight, and overall health status were monitored every other day to assess treatment effects and potential adverse reactions. Any signs of distress, severe weight loss (>20% of initial body weight), abnormal behavior, or mortality were recorded. Three days after the final treatment, tumor tissues were excised for immunohistochemical staining, and spleen lymphocytes were isolated for CTL assays and immune cell

phenotyping. Mice in the survival observation group were monitored until humane endpoints were reached, defined as a tumor volume of 2,000 mm^3 or when tumor metastasis or rapid growth caused ulceration, necrosis, or infection that impaired feeding or mobility, after which they were euthanized. After tumor regression, mice were re-challenged with the same cell line (3×10^5) on the opposite side (left) of the back, and tumor size was measured every other day. Tumor volume was calculated as volume = (length $\times$ $width^2$)/2.

Bilateral tumor model

Tumor cells (3×10^5) were injected subcutaneously on both sides of the mouse back. When the tumor diameter reached 3–5 mm (approximately 5–7 days), the mice were divided into three groups (OH2-FLT3L, OH2, and control groups), with n = 5–8 mice per group. The right-side tumor was treated. Treatment methods were as follows: (1) OH2 or OH2-FLT3L (2×10^6 pfu), administered i.t. every other day for a total of five injections; (2) PBS (100 μL) as a blank control, administered i.t. every other day for a total of five injections. Tumor diameter, mouse body weight, and overall health status were monitored every other day to assess treatment effects and potential adverse reactions. Any signs of distress, severe weight loss (>20% of initial body weight), abnormal behavior, or mortality were recorded.

Combination therapy model

Tumor cells (3×10^5) were injected subcutaneously into the right flank of mice. When the tumor diameter reached 3–5 mm (approximately 5–7 days), mice were divided into five groups: OH2-FLT3L, OH2, anti-PD1 antibody, OH2-FLT3L and anti-PD1 combination therapy, and control groups, with n = 5–10 mice per group. Treatment methods were as follows: (1) OH2 or OH2-FLT3L (2×10^6 pfu), administered i.t. every other day for five injections; (2) PBS (100 μL) as a blank control, administered i.t. every other day for five injections; (3) anti-PD1 antibody (200 μg), administered intraperitoneally (i.p.) every other day for five injections. Tumor diameter, mouse body weight, and overall health status were monitored every other day to assess treatment effects and potential adverse reactions. Any signs of distress, severe weight loss (>20% of initial body weight), abnormal behavior, or mortality were recorded.

Immunohistochemical staining

Immunohistochemistry was performed by Wuhan Servicebio Technology Co., Ltd. The following primary antibodies were used: Recombinant Anti-CD3 antibody (Rabbit mAb, Servicebio, GB151137) at a dilution of 1:1,000, Recombinant Anti-CD4 antibody (Rabbit mAb, Servicebio, GB15064) at a dilution of 1:200, Recombinant Anti-CD8 alpha antibody (Rabbit mAb, Servicebio, GB15068) at a dilution of 1:400, and Anti-CD11c Rabbit pAb (Servicebio, GB11059) at a dilution of 1:200. The secondary antibody was horseradish peroxidase-conjugated Goat Anti-Rabbit immunoglobulin (Ig)G (Servicebio, GB23303) at a dilution of 1:200.

Immunocyte flow phenotyping

Three days after the final treatment, mice (three per group) were euthanized by cervical dislocation to analyze immune cell phenotypes (DC, CD4+ T cells, CD8+ T cells, Gr-1+ CD11b+ myeloid cells, NK cells, etc.) in the spleen. Spleen lymphocytes were separated by gradient centrifugation at room temperature and washed twice with PBS. Lymphocytes from each mouse were divided into multiple staining panels and incubated on ice in the dark with the following flow cytometry antibodies (DCs: Gr-1 [FITC, 108405; BioLegend], I-A/I-E [APC, 107614; BioLegend], CD11c [PerCP, 117325; BioLegend], CD11b [PE, 101208; BioLegend]; T cell: CD3[FITC, 100204; BioLegend], CD4 [PerCP, 100432; BioLegend], CD8a [PE, 162304; BioLegend], CD44 [APC, 103012; BioLegend]; NK cell: CD3 [FITC, 100204; BioLegend], CD49b [APC/Cyanine7, 108920; BioLegend]; Gr-1+ CD11b+ myeloid cells: Gr-1 [FITC, 108405; BioLegend], CD11b [PE, 101208; BioLegend]). Flow cytometry (BD-LSRII) was performed, and results were analyzed using FlowJo.

Single-cell sequencing

Tumor tissues were isolated from the control, OH, and OH2-FLT3L groups in the CT26 mouse model 21 days after tumor inoculation for single-cell sequencing. The single-cell sequencing technology used in this study was provided by BGI. Tumor tissues were dissociated using the Tumor Dissociation Kit (Mouse, MACS) to remove dead cells, leaving a single-cell suspension of live cells for sequencing. The data obtained were analyzed by RepuGene Technology.

Statistical analysis

Statistical analyses were performed using GraphPad Prism version 8, with statistical significance set at $p < 0.05$. ELISA, flow cytometry, immunohistochemical quantification results, and tumor volume data were analyzed using Turkey's multiple comparisons test and ANOVA. Kaplan-Meier curves were used to represent animal survival, and statistical analysis was performed using the log rank (Mantel-Cox) test. Results are expressed as mean ± SEM. All experiments were performed at least three times unless otherwise stated. Ns: no significant differences; $*p < 0.05$; $**p < 0.01$; $***p < 0.001$; $****p < 0.0001$.

DATA AVAILABILITY

The data used during the current study are available from the corresponding author upon reasonable request.

ACKNOWLEDGMENTS

This study was supported by the National Key R&D Program of China (grant number: 2023YFC3403300), the Major Science and Technology Project of Hubei Province (grant number: 2022ACA001), and the Cancer Foundation of China (H092301).

AUTHOR CONTRIBUTIONS

W.Z., K.Z., and D.W. conceived and designed the experiments. D.W., Q.Z., and Z.Y. conducted the experiments. D.W., Q.Z., and W.Z. performed data processing and statistical analysis. D.W., Q.Z., and W.Z. prepared the manuscript. X.Z. and P.X. assisted in the experiments and data analysis. S.C. provided administrative and technical support. W.Z. and K.Z. supervised the study. L.X. and B.L. contributed to conceptualization and funding acquisition. All authors read and approved the final manuscript.

DECLARATION OF INTERESTS

The authors declare no competing interests.

SUPPLEMENTAL INFORMATION

Supplemental information can be found online at https://doi.org/10.1016/j.omton.2025.200975.

REFERENCES

1. Kennedy, L.B., and Salama, A.K.S. (2020). A review of cancer immunotherapy toxicity. CA Cancer J. Clin. *70*, 86–104.
2. Waldman, A.D., Fritz, J.M., and Lenardo, M.J. (2020). A guide to cancer immunotherapy: From T cell basic science to clinical practice. Nat. Rev. Immunol. *20*, 651–668.
3. Hellmann, M.D., Paz-Ares, L., Bernabe Caro, R., Zurawski, B., Kim, S.-W., Carcereny Costa, E., Park, K., Alexandru, A., Lupinacci, L., de la Mora Jimenez, E., et al. (2019). Nivolumab plus Ipilimumab in Advanced Non-Small-Cell Lung Cancer. N. Engl. J. Med. *381*, 2020–2031.
4. Abou Khouzam, R., Goutham, H.V., Zaarour, R.F., Chamseddine, A.N., Francis, A., Buart, S., Terry, S., and Chouaib, S. (2020). Integrating tumor hypoxic stress in novel and more adaptable strategies for cancer immunotherapy. Semin. Cancer Biol. *65*, 140–154.
5. Gonzalez, H., Hagerling, C., and Werb, Z. (2018). Roles of the immune system in cancer: From tumor initiation to metastatic progression. Genes Dev. *32*, 1267–1284.
6. Hanahan, D., and Weinberg, R.A. (2011). Hallmarks of cancer: The next generation. Cellule *144*, 646–674.
7. Wculek, S.K., Cueto, F.J., Mujal, A.M., Melero, I., Krummel, M.F., and Sancho, D. (2020). Dendritic cells in cancer immunology and immunotherapy. Nat. Rev. Immunol. *20*, 7–24.
8. Heras-Murillo, I., Adán-Barrientos, I., Galán, M., Wculek, S.K., and Sancho, D. (2024). Dendritic cells as orchestrators of anticancer immunity and immunotherapy. Nat. Rev. Clin. Oncol. *21*, 257–277.
9. Tiwari, A., Trivedi, R., and Lin, S.-Y. (2022). Tumor microenvironment: Barrier or opportunity towards effective cancer therapy. J. Biomed. Sci. *29*, 83.
10. Boissonnas, A., Licata, F., Poupel, L., Jacquelin, S., Fetler, L., Krumeich, S., Théry, C., Amigorena, S., and Combadière, C. (2013). CD8+ tumor-infiltrating T cells are trapped in the tumor-dendritic cell network. Neoplasia *15*, 85–94.
11. Perrot, I., Blanchard, D., Freymond, N., Isaac, S., Guibert, B., Pachéco, Y., and Lebecque, S. (2007). Dendritic cells infiltrating human non-small cell lung cancer are blocked at immature stage. J. Immunol. *178*, 2763–2769.
12. McKenna, H.J., Stocking, K.L., Miller, R.E., Brasel, K., De Smedt, T., Maraskovsky, E., Maliszewski, C.R., Lynch, D.H., Smith, J., Pulendran, B., et al. (2000). Mice lacking flt3 ligand have deficient hematopoiesis affecting hematopoietic progenitor cells, dendritic cells, and natural killer cells. Blood *95*, 3489–3497.
13. Ager, C.R., Reilley, M.J., Nicholas, C., Bartkowiak, T., Jaiswal, A.R., and Curran, M. A. (2017). Intratumoral STING activation with T-cell checkpoint modulation generates systemic antitumor immunity. Cancer Immunol. Res. *5*, 676–684.
14. Hammerich, L., Marron, T.U., Upadhyay, R., Svensson-Arvelund, J., Dhainaut, M., Hussein, S., Zhan, Y., Ostrowski, D., Yellin, M., Marsh, H., et al. (2019). Systemic clinical tumor regressions and potentiation of PD1 blockade with in situ vaccination. Nat. Med. *25*, 814–824.
15. Bickett, T.E., Knitz, M., Darragh, L.B., Bhatia, S., Van Court, B., Gadwa, J., Bhuvane, S., Piper, M., Nguyen, D., Tu, H., et al. (2021). FLT3L release by NK cells enhances response to radioimmunotherapy in preclinical models of HNSCC. Clin. Cancer Res. *27*, 6235–6249.
16. Kroemer, G., Galluzzi, L., Kepp, O., and Zitvogel, L. (2013). Immunogenic cell death in cancer therapy. Annu. Rev. Immunol. *31*, 51–72.
17. van Vloten, J.P., Workenhe, S.T., Wootton, S.K., Mossman, K.L., and Bridle, B.W. (2018). Critical Interactions between Immunogenic Cancer Cell Death, Oncolytic Viruses, and the Immune System Define the Rational Design of Combination Immunotherapies. J. Immunol. *200*, 450–458.
18. Ilkow, C.S., Swift, S.L., Bell, J.C., and Diallo, J.-S. (2014). From scourge to cure: Tumour-selective viral pathogenesis as a new strategy against cancer. PLoS Pathog. *10*, e1003836.
19. Hu, J.C.C., Coffin, R.S., Davis, C.J., Graham, N.J., Groves, N., Guest, P.J., Harrington, K.J., James, N.D., Love, C.A., McNeish, I., et al. (2006). A phase I study of OncoVEXGM-CSF, a second-generation oncolytic herpes simplex virus expressing granulocyte macrophage colony-stimulating factor. Clin. Cancer Res. *12*, 6737–6747.
20. Senzer, N.N., Kaufman, H.L., Amatruda, T., Nemunaitis, M., Reid, T., Daniels, G., Gonzalez, R., Glaspy, J., Whitman, E., Harrington, K., et al. (2009). Phase II clinical trial of a granulocyte-macrophage colony-stimulating factor-encoding, second-generation oncolytic herpesvirus in patients with unresectable metastatic melanoma. J. Clin. Oncol. *27*, 5763–5771.
21. Zhao, Q., Zhang, W., Ning, Z., Zhuang, X., Lu, H., Liang, J., Li, J., Zhang, Y., Dong, Y., Zhang, Y., et al. (2014). A Novel Oncolytic Herpes Simplex Virus Type 2 Has Potent Anti-Tumor Activity. PLoS One *9*, e93103.
22. Thapa, B., Kato, S., Nishizaki, D., Miyashita, H., Lee, S., Nesline, M.K., Previs, R.A., Conroy, J.M., DePietro, P., Pabla, S., and Kurzrock, R. (2024). OX40/OX40 ligand and its role in precision immune oncology. Cancer Metastasis Rev. *43*, 1001–1013.
23. Postow, M.A., Callahan, M.K., Barker, C.A., Yamada, Y., Yuan, J., Kitano, S., Mu, Z., Rasalan, T., Adamow, M., Ritter, E., et al. (2012). Immunologic correlates of the abscopal effect in a patient with melanoma. N. Engl. J. Med. *366*, 925–931.
24. Shalhout, S.Z., Miller, D.M., Emerick, K.S., and Kaufman, H.L. (2023). Therapy with oncolytic viruses: Progress and challenges. Nat. Rev. Clin. Oncol. *20*, 160–177.
25. Zhang, B., Huang, J., Tang, J., Hu, S., Luo, S., Luo, Z., Zhou, F., Tan, S., Ying, J., Chang, Q., et al. (2021). Intratumoral OH2, an oncolytic herpes simplex virus 2, in patients with advanced solid tumors: A multicenter, phase I/II clinical trial. J. Immunother. Cancer *9*, e002224.
26. Zhang, H., Ren, Y., Wang, F., Tu, X., Tong, Z., Liu, L., Zheng, Y., Zhao, P., Cheng, J., Li, J., et al. (2024). The long-term effectiveness and mechanism of oncolytic virotherapy combined with anti-PD-L1 antibody in colorectal cancer patient. Cancer Gene Ther. *31*, 1412–1426.
27. Anderson, K.G., Stromnes, I.M., and Greenberg, P.D. (2017). Obstacles posed by the tumor microenvironment to T cell activity: A case for synergistic therapies. Cancer Cell *31*, 311–325.
28. de Visser, K.E., and Joyce, J.A. (2023). The evolving tumor microenvironment: From cancer initiation to metastatic outgrowth. Cancer Cell *41*, 374–403.
29. Milling, L., Zhang, Y., and Irvine, D.J. (2017). Delivering safer immunotherapies for cancer. Adv. Drug. Deliv. Rev. *114*, 79–101.
30. Momenilandi, M., Lévy, R., Sobrino, S., Li, J., Lagresle-Peyrou, C., Esmaeilzadeh, H., Fayand, A., Floc'h, C.L., Guérin, A., Della Mina, E., et al. (2024). FLT3L governs the development of partially overlapping hematopoietic lineages in humans and mice. Cell *187*, 2817–2837.e31.
31. Tsapogas, P., Swee, L.K., Nusser, A., Nuber, N., Kreuzaler, M., Capoferri, G., Rolink, H., Ceredig, R., and Rolink, A. (2014). In vivo evidence for an instructive role of fms-like tyrosine kinase-3 (FLT3) ligand in hematopoietic development. Haematologica *99*, 638–646.
32. Durai, V., Bagadia, P., Briseño, C.G., Theisen, D.J., Iwata, A., Davidson, J.T., Gargaro, M., Fremont, D.H., Murphy, T.L., and Murphy, K.M. (2018). Altered compensatory cytokine signaling underlies the discrepancy between Flt3-/- and Flt3l-/- mice. J. Exp. Med. *215*, 1417–1435.
33. Guilliams, M., Ginhoux, F., Jakubzick, C., Naik, S.H., Onai, N., Schraml, B.U., Segura, E., Tussiwand, R., and Yona, S. (2014). Dendritic cells, monocytes and macrophages: A unified nomenclature based on ontogeny. Nat. Rev. Immunol. *14*, 571–578.
34. Fujita, K., Chakarov, S., Kobayashi, T., Sakamoto, K., Voisin, B., Duan, K., Nakagawa, T., Horiuchi, K., Amagai, M., Ginhoux, F., and Nagao, K. (2019). Cell-autonomous FLT3L shedding via ADAM10 mediates conventional dendritic cell development in mouse spleen. Proc. Natl. Acad. Sci. USA *116*, 14714–14723.
35. Ryschich, E., Huszty, G., Wentzensen, N., Schmidt, E., Knaebel, H.P., Encke, J., Märten, A., Büchler, M.W., and Schmidt, J. (2007). Effect of Flt3 ligand gene transfer in experimental pancreatic cancer. Int. J. Colorectal Dis. *22*, 215–223.
36. Lynch, D.H., Andreasen, A., Maraskovsky, E., Whitmore, J., Miller, R.E., and Schuh, J.C. (1997). Flt3 ligand induces tumor regression and antitumor immune responses in vivo. Nat. Med. *3*, 625–631.

37. Chakravarty, P.K., Alfieri, A., Thomas, E.K., Beri, V., Tanaka, K.E., Vikram, B., and Guha, C. (1999). Flt3-ligand administration after radiation therapy prolongs survival in a murine model of metastatic lung cancer. Cancer Res. *59*, 6028–6032.

38. Hegde, S., Krisnawan, V.E., Herzog, B.H., Zuo, C., Breden, M.A., Knolhoff, B.L., Hogg, G.D., Tang, J.P., Baer, J.M., Mpoy, C., et al. (2020). Dendritic cell paucity leads to dysfunctional immune surveillance in pancreatic cancer. Cancer. Cell. *37*, 289–307.e9.

39. Faisal, S.M., Castro, M.G., and Lowenstein, P.R. (2023). Combined cytotoxic and immune-stimulatory gene therapy using Ad-TK and Ad-Flt3L: Translational developments from rodents to glioma patients. Mol. Ther. *31*, 2839–2860.

40. Bernt, K.M., Ni, S., Tieu, A.-T., and Lieber, A. (2005). Assessment of a Combined, Adenovirus-Mediated Oncolytic and Immunostimulatory Tumor Therapy. Cancer Res. *65*, 4343–4352.

41. Ali, S., Curtin, J.F., Zirger, J.M., Xiong, W., King, G.D., Barcia, C., Liu, C., Puntel, M., Goverdhana, S., Lowenstein, P.R., and Castro, M.G. (2004). Inflammatory and Anti-glioma Effects of an Adenovirus Expressing Human Soluble Fms-like Tyrosine Kinase 3 Ligand (hsFlt3L): Treatment with hsFlt3L Inhibits Intracranial Glioma Progression. Mol. Ther. *10*, 1071–1084.

42. Umemura, Y., Orringer, D., Junck, L., Varela, M.L., West, M.E.J., Faisal, S.M., Comba, A., Heth, J., Sagher, O., Leung, D., et al. (2023). Combined cytotoxic and immune-stimulatory gene therapy for primary adult high-grade glioma: A phase 1, first-in-human trial. Lancet Oncol. *24*, 1042–1052.

43. Oba, T., Long, M.D., Keler, T., Marsh, H.C., Minderman, H., Abrams, S.I., Liu, S., and Ito, F. (2020). Overcoming primary and acquired resistance to anti-PD-L1 therapy by induction and activation of tumor-residing cDC1s. Nat. Commun. *11*, 5415.

44. Barnard, Z., Wakimoto, H., Zaupa, C., Patel, A.P., Klehm, J., Martuza, R.L., Rabkin, S.D., Curry, W.T., Jr., and Curry, W.T. (2012). Expression of FMS-like Tyrosine Kinase 3 Ligand by Oncolytic Herpes Simplex Virus Type I Prolongs Survival in Mice Bearing Established Syngeneic Intracranial Malignant Glioma. Neurosurgery *71*, 741–748.

45. Vonderheide, R.H. (2020). CD40 Agonist Antibodies in Cancer Immunotherapy. Annu. Rev. Med. *71*, 47–58.

46. Vonderheide, R.H., and Glennie, M.J. (2013). Agonistic CD40 antibodies and cancer therapy. Clin. Cancer Res. *19*, 1035–1043.

47. Yamauchi, T., Hoki, T., Oba, T., Kajihara, R., Attwood, K., Cao, X., and Ito, F. (2022). CD40 and CD80/86 signaling in cDC1s mediate effective neoantigen vaccination and generation of antigen-specific CX3CR1+ CD8+ T cells. Cancer Immunol. Immunother. *71*, 137–151.

48. Garris, C.S., Arlauckas, S.P., Kohler, R.H., Trefny, M.P., Garren, S., Piot, C., Engblom, C., Pfirschke, C., Siwicki, M., Gungabeesoon, J., et al. (2018). Successful anti-PD-1 cancer immunotherapy requires T cell-dendritic cell crosstalk involving the cytokines IFN-γ and IL-12. Immunity *49*, 1148–1161.e7.

49. Teijeira, A., Garasa, S., Luri-Rey, C., de Andrea, C., Gato, M., Molina, C., Kaisho, T., Cirella, A., Azpilikueta, A., Wculek, S.K., et al. (2022). Depletion of Conventional Type-1 Dendritic Cells in Established Tumors Suppresses Immunotherapy Efficacy. Cancer Res. *82*, 4373–4385.

50. Zhuang, X.f., Zhou, A.p., Shi, G.l., Han, X.p., Li, J., Zhang, Y., Zhang, Y., Zhang, S.r., and Liu, B.l. (2012). [Generation of a herpes simplex virus-permissive mouse melanoma cell line B16RHSV]. Zhonghua Zhongliu Zazhi *34*, 187–191.

51. Wang, Y., Zhou, X., Wu, Z., Hu, H., Jin, J., Hu, Y., Dong, Y., Zou, J., Mao, Z., Shi, X., et al. (2019). Preclinical Safety Evaluation of Oncolytic Herpes Simplex Virus Type 2. Hum. Gene Ther. *30*, 651–660.

52. Zhu, Y., Hu, X., Feng, L., Yang, Z., Zhou, L., Duan, X., Cheng, S., Zhang, W., Liu, B., and Zhang, K. (2019). Enhanced Therapeutic Efficacy of a Novel Oncolytic Herpes Simplex Virus Type 2 Encoding an Antibody Against Programmed Cell Death 1. Mol. Ther. Oncolytics *15*, 201–213.

53. (1992). Generation of large numbers of dendritic cells from mouse bone marrow cultures supplemented with granulocyte/macrophage colony-stimulating factor. J. Exp. Med. *176*, 1693–1702.